Complete thermodynamically consistent kinetic model of particle nucleation and growth: Numerical study of the applicability of the classical theory of homogeneous nucleation

Evgeni N. Chesnokov and Lev N. Krasnoperov[a)]
Department of Chemistry and Environmental Science, New Jersey Institute of Technology, Newark, New Jersey 07102 and Institute of Chemical Kinetics and Combustion, Novosibirsk 630090, Russia

(Received 6 November 2006; accepted 22 January 2007; published online 10 April 2007)

A complete thermodynamically consistent elementary reaction kinetic model of particle nucleation and growth from supersaturated vapor was developed and numerically evaluated to determine the conditions for the steady-state regime. The model treats all processes recognized in the aerosol science (such as nucleation, condensation, evaporation, agglomeration/coagulation, etc.) as reversible elementary reactions. It includes all possible forward reactions (i.e., of monomers, dimers, trimers, etc.) together with the thermodynamically consistent reverse processes. The model is built based on the Kelvin approximation, and has two dimensionless parameters: S_0—the initial supersaturation and Θ—the dimensionless surface tension. The time evolution of the size distribution function was obtained over the ranges of parameters S_0 and Θ. At low initial supersaturations, S_0, the steady state is established after a delay, and the steady-state distribution function corresponds to the predictions of the classical nucleation theory. At high initial supersaturations, the depletion of monomers due to condensation on large clusters starts before the establishing of the steady state. The steady state is never reached, and the classical nucleation theory is not applicable. The boundary that separates these two regimes in the two dimensionless parameter space, S_0 and Θ, was determined. The model was applied to several experiments on water nucleation in an expansion chamber [J. Wolk and R. Strey, J. Phys. Chem. B **105**, 11683 (2001)] and in Laval nozzle [Y. J. Kim *et al.*, J. Phys. Chem. A **108**, 4365 (2004)]. The conditions of the experiments performed using Laval nozzle (S_0=40–120) were found to be close to the boundary of the non-steady-state regime. Additional calculations have shown that in the non-steady-state regime the nucleation rate is sensitive to the rate constants of the initial steps of the nucleation process, such as the monomer-monomer, monomer-dimer, etc., reactions. This conclusion is particularly important for nucleation from supersaturated water vapor, since these processes for water molecules at and below the atmospheric pressure are in the low pressure limit, and the rate constants can be several orders of magnitude lower than the gas kinetic. In addition, the impact of the thermodynamic inconsistency of the previously developed partially reversible kinetic numerical models was assessed. At typical experimental conditions for water nucleation, S_0=10 and Θ=10 (T=250 K), the error in the particle nucleation rate introduced by the thermodynamic inconsistency exceeds one order of magnitude. © *2007 American Institute of Physics*.
[DOI: 10.1063/1.2672647]

INTRODUCTION

Numerical modeling is widely used in studies of particle nucleation and growth from supersaturated solutions (such as in aerosol formation, phase transitions, etc.). For a period of time, an analytical approach known as the classical nucleation theory was used to describe the nucleation dynamics.[1–4] Later, numerical models of the kinetics of particle nucleation and growth have been developed.[5–8] Courtney applied a kinetic model to a non-steady-state nucleation of water vapor.[5] Mazlovsky used numerical approach to address the problem of ferric oxide aerosol formation.[6] McMurry and Friedlander employed a numerical model to study the formation of photochemical smog,[7] and Gelbard and Seinfeld for the formation and growth of a sulfuric acid/water aerosol in a smog chamber.[8] In the pioneering work Courtney numerically solved 100 ordinary differential equations that correspond to each particle size to describe the earlier stages of nucleation.[5] In the further studies to incorporate larger particle sizes, a technique based on the division of the particle size domain into sections was used.[6,8–10] Subsequently the numerical modeling was used to interpret the nucleation of magnesium oxide particles,[11,12] silicon dioxide,[13] and formation of aerosol particles in photochemical decomposition of tungsten hexacarbonyl and halobenzenes.[14]

The kinetic models used in these studies could be divided into two groups.[15] In the first group are the coagulation models, which contain only irreversible monomer-cluster and cluster-cluster addition reactions. Such models are used

[a)]Author to whom correspondence should be addressed. Electronic mail: krasnoperov@adm.njit.edu

for very large supersaturations (such as for substances with very low vapor pressures), when the reverse processes (evaporation of large particles as well as dissociation of small clusters down to the trimers and dimers) can be neglected. The nucleation models that contain both condensation and evaporation of monomers belong to the second group. The rate constants of the forward processes are calculated either based on the kinetic theory of gases in the free molecular regime, or on the Brownian motion when reactions are diffusion controlled. The rate constants for the monomer evaporation are calculated using the Kelvin formula for the vapor pressure above a spherical surface.

In several studies, the coagulation and nucleation models were combined.[11,16–19] In these combined models, in addition to the monomer-cluster and cluster-cluster association reactions, evaporation of monomers from clusters is also taken into account. In Friedlander's book[10] this model is tagged as the "general dynamic equation." The model was applied to sulfuric acid and water aerosol formation,[16] particle formation in pyrolysis of silanes,[19–21] condensation of magnesium oxide,[11] a model aerosol nucleation,[17] and in a numerical investigation of different types of aerosol reactors.[18]

The general dynamic equation model is only partially reversible as it takes into account only the reverse reaction for the monomer condensation and does not take into account the reverse reaction for the cluster-cluster coagulation. A standard justification for not accounting the processes of evaporation of dimers, trimers, etc., is that the evaporation of dimers, trimers, etc., from large particles can be neglected being much slower than the evaporation of monomers. This is certainly true for large particles. However, the same assumption is extended to small clusters, which requires justification. The errors associated with this neglecting are difficult to assess. The partially reversible models have an inherent problem—they are thermodynamically inconsistent due to violation of the principle of detailed balance. The resulting system of differential equations does not have a solution that corresponds to the thermodynamically equilibrium state. Intuitively, it appears to be not important for systems that are far from equilibrium, however, the range of the conditions where such thermodynamic inconsistency plays a role is yet to be assessed.

On the other hand, a complete kinetic model which treats all reaction (cluster-cluster and cluster-monomer) as reversible does not require any additional parameters beyond those used in the partially reversible models. The rate constants for the evaporation of dimers, trimers, etc., can be derived based on the rate constant for the monomer evaporation using the principle of detailed balance. Katz *et al.*[22] used this approach to find corrections to classical nucleation theory due to condensation and evaporation of dimers, trimers, etc. Recently Arstila[23] assessed the impact of the evaporation of dimers, trimers, etc., on the steady-state cluster size distribution function and the nucleation rate. It should be noted that such an approach is generally accepted in the modeling complex chemical reactions, where kinetic models use detail balanced elementary reactions, which require the rate constants in the forward directions as well as the thermodynamic properties of the reactants and products. The rate constants for the reverse reactions are calculated based on the equilibrium constants determined from the thermochemical data.

In this work a complete thermodynamically consistent kinetic model for particle nucleation and growth was developed. The kinetic model was converted into a computer code via a sectioning (binning) procedure. The code itself can be used for a wide range of problems, such as the initial phase of aerosol formation process or the final phase of particle coagulation, as well as for different experimental arrangements, such as continuous or pulsed monomer production. In the current research, in the majority of the calculations, the free molecular condensation for the forward processes combined with the Kelvin model (the surface tension model) to calculate the reverse processes was used. However, the set of the rate constants as well as the thermodynamic properties can be varied to incorporate any deviations from the free molecular condensation and the surface tension model. Additional calculations were performed with a reduced (compared to the gas kinetic) rate constant of the dimer formation to assess the impact of the "pressure falloff" effects in the dimerization of water.

All versions of the classical nucleation theory[1,2,4,24] assume the existence of the steady-state regime, which is used to calculate the nucleation rate. Such a steady state does not necessarily exist. The establishing of the steady state requires time. The problem of the time lag was thoroughly addressed.[21,25] However, there is another time limit for the existence of the steady state. After establishing, the steady state survives until the onset of rapid condensation of monomers on growing particles. This fast condensation destroys the steady-state distribution functions. The larger the supersaturation, the shorter is the time delay before this massive condensation. This delay might become shorter than the time lag for the establishing of the steady state. In this case the nucleation occurs not in the steady-state regime, and the classical nucleation theory is not applicable anymore.

The second issue that is addressed in this study is the possible errors associated with the thermodynamic inconsistency of the partially reversible kinetic models of particle nucleation and growth. It is shown that under some experimental conditions (easily encountered in practice) such thermodynamic inconsistency can lead to significant (from one to several orders of magnitude) errors in the concentrations of critical nuclei, and, hence, in the nucleation rates.

In the current study, for the purpose of comparison, the same approximations for the collision rate constants and the thermodynamic parameters as in the classical nucleation theory are made. As in the classical nucleation theory and in the previous kinetic models, for the cluster-cluster reactions the rate constants based on the gas collision theory (free molecular condensation) are used. The rate constants for the reverse reactions are calculated based on the Gibbs free energies of clusters formation from monomers, which in turn are based on the Kelvin formula for the vapor pressure above curved surfaces (the surface tension model).

There are several versions of the nucleation theory that differ somewhat by the expressions used for thermodynamic parameters of the clusters based on the same initial Kelvin formula.[3,24,26,27] These differences are associated with the

different level approximations made in the derivation of the thermodynamic expressions. The critical survey on the issue is given by Wilemski.[28] The classical nucleation theory uses the expression that is in conflict with the law of mass action.[28] Courtney noted and corrected this contradiction.[5] Currently, the correction introduced by Girshick and Chiu[26] is widely used, where the Gibbs free energies for all clusters are rather arbitrary shifted to set the Gibbs free energy of formation of a monomer from monomers to zero. Katz[27] introduced an expression for the Gibbs free energy of formation of clusters from monomers via a sum of terms that reflect sequential additions of monomers. This expression is free of inconsistencies associated with other expressions[28] and, perhaps, is the most natural in association with the Kelvin model. This expression (hereafter "the discrete Kelvin model") is adopted in this study for the description of the thermodynamic properties of clusters. Wilemski[28] showed that the difference between the discrete Kelvin model and the classical expression corrected by Girshick and Chiu[26] is not significant.

As it was already mentioned, we focus our discussion on two issues—the numerical verification of the assumption of the steady state and the assessment of the potential impact of the "kinetic cycles" caused by the thermodynamic inconsistency of the combined models. It should be stressed that it is not our intention to discuss the validity of the thermodynamic properties of clusters derived based on the Kelvin model, which was done in numerous previous works.[28] The Kelvin model is used in this study only for the reason that the large body of the previous studies as well as the interpretations of the experiments are based on this model. The numerical model developed and evaluated in the current work can be used with any set of thermodynamic parameters, such as derived, for example, using theoretical chemistry.[29] The rate constants in the model could be incorporated from different sources as well. For example, the rate constants calculated using variational transition state theory could be used.[30] Although we use the simple gas kinetic model for the forward rate constants, it is realized that the rate constants for the dimerization (and even subsequent formation of trimers, etc.) of small molecules (such as water) might be in the low pressure or in the pressure falloff region, therefore being quite different from the gas kinetic rate constants or the rate constants calculated using any form of the transition state theory. In addition, it should be noted that another purpose of the study was to investigate the applicability of classical approaches to the systems in extreme conditions, such as with very large supersaturations achieved in the nanoparticle formation by rapid expansion of supercritical solutions,[31] condensation of supercooled vapors after the Laval nozzle,[32] as well as in the pulsed initiation of photochemical aerosols.[33] In all these examples the initial supersaturations are from ~50–150 (Ref. 32) to $>10^9$.[31] Due to the nature of these experiments, we use the initial value formulation of the problem, that is, the time evolution of the size distribution function is calculated starting from instantly generated monomers. Furthermore, several comparisons are made with the experimental data and the predictions of the classical nucleation theory for condensation of water under more "benign" conditions of typical nucleation experiments.

KINETIC MODEL

While in the particle nucleation and growth terminology the processes are separated into "nucleation," "condensation," "agglomeration," "coagulation," etc., in our approach, we treat all processes similarly as reversible elementary reactions of clusters consisting of n monomers with clusters consisting of m monomers,

$$P_n + P_m \rightleftharpoons P_{n+m}, \quad n,m = 1,2,3, \ldots \infty. \tag{1}$$

The set of elementary reactions [Eq. (1)] results in the ordinary differential equation (ODE) system

$$\frac{dN_n}{dt} = -\sum_{m=1}^{\infty} \nu_{nm}(k_{nm}N_nN_m - k'_{nm}N_{n+m}) + \sum_{m+k=n,m\geq k} \nu'_{mk}(k_{mk}N_mN_k - k'_{nm}N_n), \tag{2}$$

where k_{nm} and k'_{nm} are the rate constants of reaction (1) in the forward and reverse directions, and ν_{nm} and ν'_{mk} are the stoichiometric coefficients,

$$\nu_{nm} = 2 \quad \text{for } n = m,$$
$$\nu_{nm} = 1 \quad \text{for } n \neq m, \tag{3}$$
$$\nu'_{mk} = 1 \quad \text{for any } m \text{ and } k.$$

N_n(molecule cm^{-3}) is the number density of clusters consisting of n monomers, and k_{nm}(cm^3 molecule^{-1} s^{-1}) and k'_{nm}(s^{-1}) are the rate constants for the forward and reverse reactions [Eq. (1)] respectively.

The reverse rate constants are determined based on the forward rate constants, k_{nm}, and the equilibrium constants of reaction (1) according to the principle of detailed balance. The equilibrium constants are calculated based on the "discrete Kelvin model."[27,28] The details of the derivation are given in Appendix A. The rate constants of the reverse reactions, k'_{nm}, are given by

$$k'_{nm} = k_{nm}\left(\frac{P^{\theta}N_A}{RT}\right)\left(\frac{p_1^*}{p^{\theta}}\right) \times \exp\left(\frac{2\Theta}{3}\left(\sum_{i=2}^{n+m}\frac{1}{i^{1/3}} - \sum_{i=2}^{n}\frac{1}{i^{1/3}} - \sum_{i=2}^{m}\frac{1}{i^{1/3}}\right)\right), \tag{4}$$

where p_1^* is the equilibrium vapor pressure above a flat surface, p^{Θ}=1 bar is the standard pressure, N_A is Avogadro's number, R is the gas constant, and Θ is the dimensionless surface energy of a monomer,[26]

$$\Theta = \frac{4\pi r_1^2\gamma}{k_BT} = \frac{\pi^{1/3}(6V_1)^{2/3}\gamma}{k_BT}. \tag{5}$$

Here V_1 is the volume of the monomer, r_1 is the radius of the monomer, γ is the surface tension, and k_B is Boltzmann's constant. Both the monomer volume V_1 and the radius r_1 are defined by

$$V_1 = V_{m,1}/N_A = (4\pi/3)r_1^3, \tag{6}$$

where $V_{m,1}$ is the molar volume of the monomer in the condensed phase. Throughout the paper we define the supersaturation as the ratio of the *concentrations of monomers*, not through the ratio of partial vapor pressures.[15,28] The supersaturation defined in this way is approximately equal to the supersaturation calculated using the partial vapor pressures,

$$S_0 \equiv \frac{N_{1,0}}{N_1^*} \approx \frac{p_0}{p^*}, \tag{7}$$

where S_0 is the initial supersaturation, $N_{1,0}$ is the initial number density of the monomers, N_1^* is the equilibrium number density of monomers above a flat surface, p_0 is the initial partial pressure of the vapor, and p^* is the equilibrium vapor pressure above a flat surface.

Equation (4) can be transformed as

$$k'_{nm} = k_{nm} N_1^* \exp\left(\frac{2\Theta}{3}\left(\sum_{i=2}^{n+m}\frac{1}{i^{1/3}} - \sum_{i=2}^{n}\frac{1}{i^{1/3}} - \sum_{i=2}^{m}\frac{1}{i^{1/3}}\right)\right). \tag{8}$$

In this work we refer to the pulsed arrangement of the experiment, when the supersaturation of the monomers is achieved on a time scale much shorter than the characteristic time of all subsequent reactions, including the reaction of dimerization. Therefore, for the system of ODE system (2) the initial conditions are

$$N_1 = N_{1,0}, \quad N_2 = N_3 = N_4 = \cdots = 0 \quad \text{at } t = 0. \tag{9}$$

The ODE system (2) is further transformed by introducing dimensionless variables, specifically dimensionless time, τ, and dimensionless number densities, n_i,

$$\tau = t 2k_{11} N_{1,0}, \tag{10}$$

$$n_i = N_i/N_{1,0}. \tag{11}$$

The system of Eq. (2) becomes

$$\frac{dn_n}{d\tau} = -\sum_{m=1}^{\infty} \nu_{nm}(\kappa_{nm} n_n n_m - \kappa'_{nm} n_{n+m}) + \sum_{m+k=n, m\geq k} \nu'_{mk}(\kappa_{mk} n_m \cdot n_k - \kappa'_{mk} \cdot n_n). \tag{12}$$

The dimensionless initial conditions are

$$n_1 = 1, \quad n_2 = n_3 = n_4 = \cdots = 0 \quad \text{at } t = 0. \tag{13}$$

The new dimensionless rate constants in Eq. (12) are defined as

$$\kappa_{nm} = k_{nm}/2k_{11}, \tag{14}$$

$$\kappa'_{nm} = k'_{nm}/2N_{1,0}k_{11}. \tag{15}$$

In the gas kinetic model (free molecular condensation) the dimensionless rate constants are[10] (note that we use the definitions accepted in chemical kinetics, where for reaction of two identical molecules the stoichiometric coefficient of 2 appears in the differential equation with simultaneous reduction of the gas collision rate constant by a factor of 2),

$$\kappa_{nm} = \frac{1}{\nu_{nm}}\frac{1}{4\sqrt{2}}(n^{1/3} + m^{1/3})^2(1/n + 1/m)^{1/2}. \tag{16}$$

For the dimensionless rate constant of the reverse reaction, combining Eqs. (4), (7), and (8), one obtains

$$\kappa'_{nm} = \kappa_{nm}\left(\frac{1}{S_0}\right)\exp\left(\frac{2\Theta}{3}\left(\sum_{i=2}^{n+m} i^{-1/3} - \sum_{i=2}^{n} i^{-1/3} - \sum_{i=2}^{m} i^{-1/3}\right)\right), \tag{17}$$

where S_0 is defined in Eq. (7).

Finally, the dimensionless problem consists of the set of ordinary differential equations [Eq. (12)] with the initial conditions [Eq. (13)] and the dimensionless rate constants [Eqs. (16) and (17)]. The problem has two dimensionless parameters, the initial supersaturation S_0 and the dimensionless surface energy of a monomer, Θ. The first parameter S_0 is the ratio of the initial concentration of monomers and the equilibrium concentration of monomers in saturated vapor above flat surface. Under the approximation made (negligible contribution of dimers, trimers, etc., to the vapor pressure above a flat surface) this parameter is equal to the ratio p_0/p^*. The second parameter Θ is the ratio of the surface energy of a monomer and the characteristic thermal energy k_BT. This parameter depends on the surface tension and temperature. For reference, the initial critical nucleus size $n_{c,0}$ is expressed via S_0 and Θ,[4]

$$n_{c,0} = \left(\frac{2\Theta}{3\ln S_0}\right)^3. \tag{18}$$

NUMERICAL APPROACH

The number of differential equations that should be taken into account in Eq. (12) is determined by the maximum particle size of interest (in our calculations about 10^7). The problem cannot be solved unless further approximations are made. Several techniques for solution of large systems of differential equations have been explored. Among them are the discrete size section methods,[8,34] the moments method,[9,35] and the cubic spline method.[36] The section method is the one that is used most often. A disadvantage of the section method is the "numerical diffusion" which spreads the particle size distribution over a wider size interval. Various calculation schemes were investigated to reduce numerical diffusion.[19] Another way to circumvent this problem is in using a larger number of sections.

In this work we used the simplest form of a discrete-sectional model, but with much narrower sections. The total range of the cluster sizes from monomers to the maximum size is divided into N sections (bins). The clusters within the same section are treated as identical. The system of sections is characterized by a small number, ε. The width of the kth section is

TABLE I. Physical parameters of water used in examples 1-3.

	T, K	σ, dyn/cm	ρ, g/cm^3	Θ	S_0	P_{vapor} Pa	$N_{1,0}$ cm^{-3}	$1/2k_{11}N_{1,0}$ s	$n_{c,o}$	p_{exp} mbar
1	252	78.05	0.9922	10.57	10	31.05	8.93×10^{16}	3.11×10^{-8}	28.7	400-700
2	230	81.22	0.97	12.16	40	4.16	5.24×10^{16}	5.46×10^{-8}	10.62	0.86-6.1
3	210	83.45	0.9463	13.91	120	0.434	1.795×10^{16}	1.64×10^{-7}	7.28	0.86-6.1

$$W_k \leqslant 1 + \varepsilon L_k, \tag{19}$$

where L_k is the average cluster size in the kth section. Typically in the calculations $\varepsilon=0.01$ was used. In this case the widths of the first 100 sections are equal to 1 and they form a discrete region. In this region the differential equations for the bin concentrations coincide with the equations for the cluster concentrations. The next 50 sections then have the width $W_k=2$, and so on. The number of differential equations of the reduced (binned) system is equal to the number of sections N. The number of sections required to cover the particle size range from 1 to 10^7 is then $N=1250$ (for $\varepsilon=0.01$). It should be noted that in our calculations the sections were much narrower than that used previously. For example, $\varepsilon=0.01$ corresponds to 690 bins/decade of the cluster diameter, while in Ref. 37 only 9 sections/decade were used.

The system of differential equations [Eq. (12)] was further transformed in terms of the bin concentrations. The procedure is described in Appendix B. The resulting system of differential equations was solved numerically. The system is stiff, and implicit methods are required. The implicit Rosenbrock method with the automatic step size adjustment was used.[38] Several test calculations were performed in order to assess the accuracy of the approximations and the accuracy of the numerical calculations.

In one test we used a known exact analytical solution for the irreversible problem in a special case when all $\nu_{nm}\kappa_{nm}=1$ and $\kappa'_{nm}=0$. The solution is[10]

$$n_n(t) = \left(\frac{2}{t+2}\right)^2\left(\frac{t}{t+2}\right)^{n-1}. \tag{20}$$

For these test calculations the system of bins with $\varepsilon=0.005$ was used, with the number of equations of 2000. Comparison of the numerical solution with the analytical expression (20) resulted in the relative accuracy of 10^{-4} for the main part of the distribution function. The accuracy in the "tail" of the distribution function (where the distribution drops abruptly) was better than 0.005 (0.5%).

In another test a comparison of a numerical solution of a binned system with the numerical solution of the original large system of differential equations [Eq. (12)] was made. A system of 10 500 equations was solved numerically for dimensionless times $\tau<3000$ (for longer times the truncation of the system has an impact on the solution). Comparison with the solution of the binned system showed the accuracy in the range of 0.001–0.01 (0.1%–1%).

As a routine test of the accuracy we used numerical calculations using two different bin size systems implemented on the original system of 10^7 differential equations. Negligible difference was seen between numerical solutions performed using binning with $\varepsilon=0.005$ and $\varepsilon=0.01$. The distribution functions calculated with $\varepsilon=0.01$ and $\varepsilon=0.02$ differ by 0.2%–0.5% for the cluster concentrations in the range of $1-10^{-9}$. For the lower concentrations (at the tail of the distribution function) the differences were ~10%–20%.

In addition, conservation of the total mass in the calculations was checked. The mass disbalance increased from 0 at the start of the calculations to ~0.2%–1% at the end of the calculations (at the dimensionless time of $\tau\approx10^4$).

NUMERICAL MODELING OF PARTICLE NUCLEATION: THE CRITERION FOR THE STEADY STATE

As a test object, we first considered a model system with the parameters that correspond to supersaturated water vapor at $T=252$ K. The relevant physical properties of water for this and subsequent examples are summarized in Table I.[39] At 252 K the surface tension, the density, and the vapor pressure of water are 78.05 dyn/cm, 0.9922 g/cm^3, and 31.05 Pa, respectively. The corresponding dimensionless parameter $\Theta=10.57$. For model calculations the initial supersaturation was taken as $S_0=10$. Although these are the only parameters required for the numerical calculations, the correspondence between the dimensionless variables and the physical variables is given below for reference. The initial concentration of monomers is 8.93×10^{16} molecule cm^{-3}. This corresponds to one unit of the dimensionless concentration. The rate constant $k_{1,1}=1.8\times10^{-10}$ cm^3 molecule^{-1} s^{-1}. One unit of the dimensionless time corresponds then to 3.1×10^{-8} s. The critical nucleus size at this supersaturation is $n_{c,0}=28.7$.

The results of the numerical calculations for example 1 are shown in Figs. 1–3. Figure 1 shows the time evolution of the dimensionless distribution function. According to the initial conditions, at $\tau=0$ only monomers exist. Then the steady-state distribution establishes and spreads to larger and larger clusters. At $\tau=10$, the steady-state distribution is in the size range of 1–20, at $\tau=100$ the steady state extends to the 1–300 range, and at $\tau=400$ the steady-state distribution reached sizes larger than 10 000. The concentration of the monomers changes insignificantly during this period. The concentration of the monomers decreases quickly from the initial value $n_1=1.0$ to $n_1=0.9279$ due to the formation of dimers and trimers, and then stabilizes.

The main quantitative characteristic in the classical nucleation theory is the nucleation rate (in other words, the particle flux J_k) in the steady state. The particle flux is defined by Becker and Doring[1] as

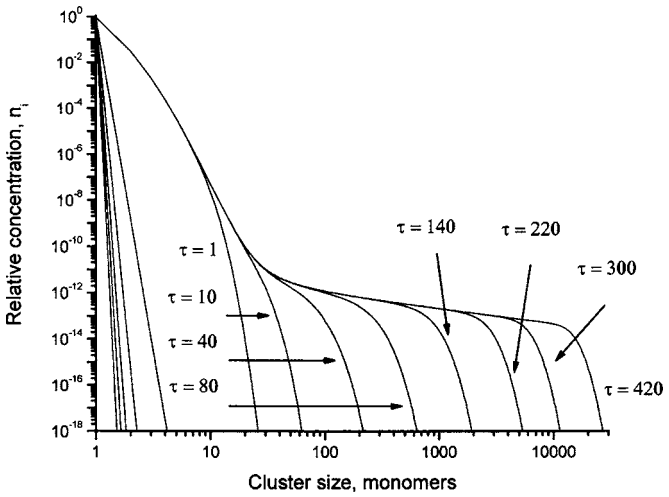

FIG. 1. Calculated dimensionless distribution functions of the cluster size. Conditions are as for example 1, Table I. Note that n_i are the concentrations of clusters of specific sizes, i.

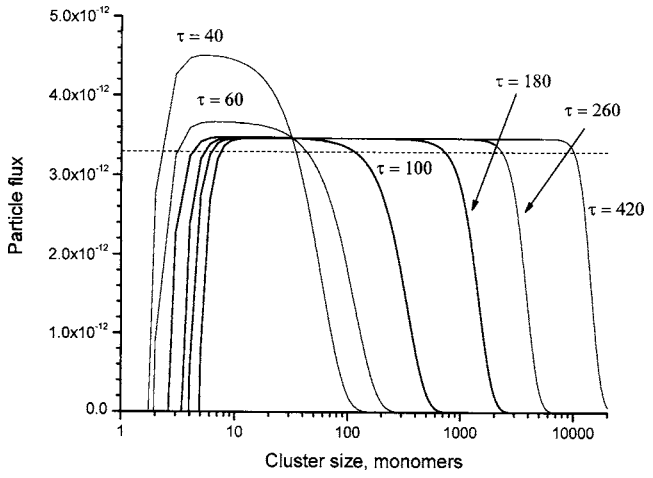

FIG. 2. The cluster flux profiles, J_k, at different dimensionless times, τ. The dashed line—the flux calculated using the classical theory of homogeneous nucleation. Conditions as in example 1, Table I.

$$J_k = J_k^+ - J_{k+1}^-, \tag{21}$$

where J_k^+ is the number of clusters which increase their size from k monomers to $(k+1)$ monomers per unit time due to the vapor condensation, and J_{k+1}^- is the number of clusters which decrease their size from $(k+1)$ monomers to k monomers per unit time due to the cluster evaporation. In the cluster size domain where the steady state exists, J_k is independent of k, $J_k=J$.

In the present kinetic model all processes of condensation/evaporation of monomers, dimers, trimers, etc., are included. Therefore, instead of Eq. (21) we define the particle flux J_k as

$$J_k = \frac{d}{dt}\sum_{i=k}^{\infty} N_i. \tag{22}$$

Definitions (21) and (22) are equivalent until the onset of coagulation of large clusters. This difference is not important because the classical nucleation theory was intended to describe the early stages of the particle nucleation and growth processes, when monomers in excess of the equilibrium concentration are still available and large clusters are still absent.

The cluster flux profiles J_k, calculated using expression (22) at different dimensionless times τ, are shown in Fig. 2. The calculations show that the steady-state distribution, which is established after a period of time, corresponds to the constant cluster flux in compliance with the classical nucleation theory. The flux profiles become rectangular shaped with the flat top at about $\tau=70$, and this shape remains until the onset of fast condensation of monomers. In this specific example condensation begins at $\tau=2500$. The constant flux during this period does not depend on time; in this example the flux is 3.46×10^{-12} in the dimensionless variables.

On the other hand, the cluster flux can be calculated using the theory of homogeneous nucleation, and compared with the numerical modeling results. To calculate J we used the exact solution of Katz and Wiedersich,[40]

$$J = \left(\sum_{q=1}^{G-1} \frac{(N_1^e)^q}{k_{q,1}N_q^e N_1^{q+1}}\right)^{-1}, \tag{23}$$

where G is a sufficiently large number, so that $(N_G/N_G^e)(N_1^e/N_1)^G \ll 1$. Expression (23) is derived from Katz formula by replacing the rate of condensation of monomers with the equivalent term, $k_{q,1}N_1N_q^e$. After substitution the parameters S_0 and Θ and conversion to the dimensionless form expression (23) becomes

$$J = \left(\sum_{q=1}^{G-1} \frac{1}{\kappa_{q,1}S_0^{q-1}n_1^{q+1}\exp\left(-(2\Theta/3)\sum_{i=2}^{q} i^{-1/3}\right)}\right)^{-1}. \tag{24}$$

Calculations were performed using the numerically stable algorithm described by Wilemski.[28] With the following parameters: $n_1=0.9279$ (which is the concentration of monomers at the dimensionless time $\tau=100$), $S_0=10$, and $\Theta=10.57$, Eq. (24) results in the dimensionless flux $J=3.29\times10^{-12}$. This value is shown by the dashed line in Fig. 2. It is slightly lower than that obtained in the numerical modeling. The difference is due to the contribution of the dimers, trimers, etc., to the condensation rate, the processes that are not taken into account in the classical nucleation theory.

After converting dimensionless J to physical units one obtains the nucleation rate of 1×10^{13} particle cm^{-3} s^{-1}. The experimental value at these conditions is about 10^4 times smaller, 7×10^8 particle cm^{-3} s^{-1}.[39] The theoretical value could be somewhat improved towards the experimental by taking into account the accommodation coefficient for water molecules in collision with liquid water. According to Li *et al.*,[41] the accommodation coefficient varies from 0.17 to 0.32 in the temperature range of 280–258 K. After this correction the difference in nucleation rates remains about 4000 times, which probably indicate the accuracy of the Kelvin model (the surface tension model) for the thermodynamics of water clusters near the critical size.

If the dimensionless parameter Θ is treated as a formal parameter of the model, it can be adjusted to fit the experi-

mental nucleation rate. In the above example *l*, it requires $\Theta=11.56$ instead of 10.57. In other words, the standard Gibbs energy of formation of the critical water cluster ($n_c=28.7$) from monomers should be ~9% larger than that predicted by the Kelvin model. This is in line with the recent comparison of modern corrected "self-consistent" theory of nucleation with the experimental data—using the Kelvin model for the thermodynamics of water cluster leads to overestimation of the nucleation rate by three to four orders of magnitude.[39]

It is instructive to compare the steady-state distribution function obtained using the present complete numerical model with the distribution function provided by the classical nucleation theory. The method for calculation of the steady-state distribution function in the classical nucleation theory in the discrete formulation is taken from Katz and Wiedersich.[40] The method is based on the recursive relationship

$$J = k_{g,1}N_gN_1 - k'_{g,1}N_{g+1}, \quad g = 1,2,3, \ldots . \tag{25}$$

For known flux J, N_2 is linked to N_1 by the first equation, N_3 is linked to N_2 by the second, and so on. However, direct implementation of this algorithm leads to problems due to a numerical instability. A stable algorithm is described by Wilemski.[28] Note that the distribution functions obtained in this way should be truncated at some large cluster size, since the distribution function extended to infinite cluster size cannot be normalized.

The comparison of the steady-state distribution functions from the present complete kinetic model with the distribution function from the nucleation theory is shown in Fig. 3. In the cluster size range of 1–30 the two curves are indistinguishable. For larger clusters the distribution functions differ; however, the difference is quite small, about 5%–10%. This example shows that for systems with moderate nucleation rates the complete kinetic model predicts almost the same nucleation rate as the correctly formulated classical nucleation theory based on the same cluster thermodynamics. The minor differences are due to the small contributions of the processes involving dimers and trimers.

The second example is a system with a high nucleation rate. In the following discussion, we refer to the experiments of Kim *et al.*[32] on water nucleation in a supersonic Laval nozzle. In these experiments, the range of supersaturations spanned from ~40 to 120. In the second example the smallest supersaturation in these experiments is considered. The experimental conditions are $T=230$ K and $S_0=40$ (example 2, Table I). The corresponding dimensionless parameters are $\Theta=12.16$ and $S_0=40$. The initial critical nucleus size at these conditions is $n_{c,0}=10.62$.

The modeling results are shown in Figs. 4–6. The time evolution of the dimensionless distribution function is shown in Fig. 4. The time dependence of the concentrations of monomers, dimers, and the 11-mers is shown in Fig. 5. Figure 6 shows the particle flux profiles at different dimensionless times.

The steady-state distribution is established at about $\tau=10$. In contrast with the previous example, the steady state exists in a relatively narrow time interval. At $\tau=100$ condensation of monomers begins. The distribution at $\tau=200$ illustrates how the condensation destroys the steady state. Finally, at $\tau=2000$ the distribution function corresponds to the mixture of slightly supersaturated vapor with growing particles. Further evolution of the distribution function is controlled by the evaporation of small particles and condensation on large particles (the Lifshitz-Slyozov regime).[42]

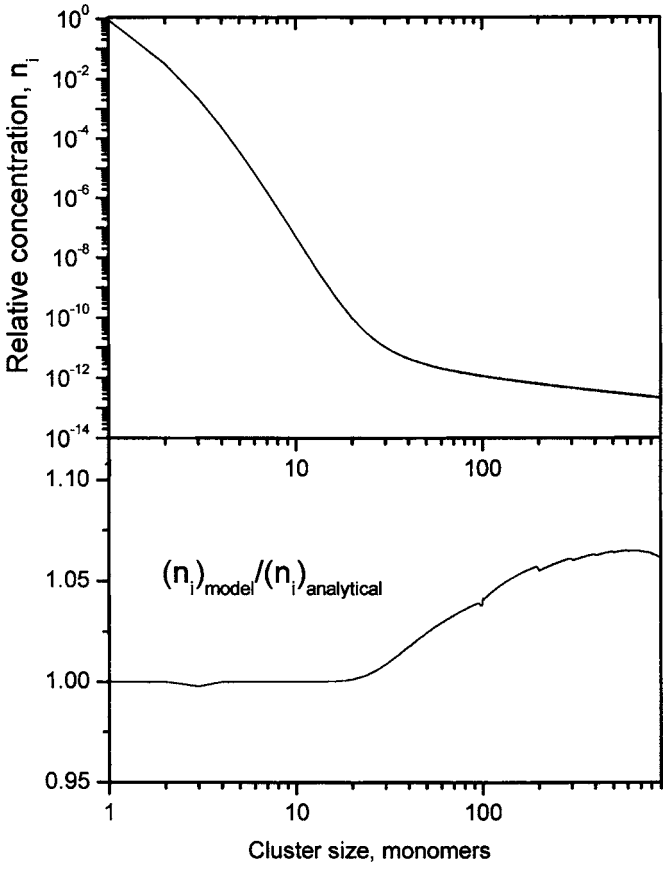

FIG. 3. The steady-state distributions calculated numerically (at $\tau=100$) and analytically (overlapped curves in the top) and their ratio (bottom). The conditions as in example 1, Table I.

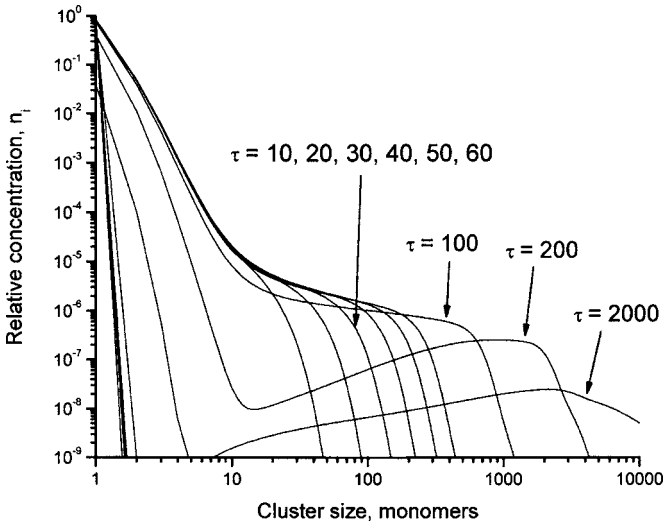

FIG. 4. Dimensionless distribution functions at different times. Conditions as in example 2, Table I.

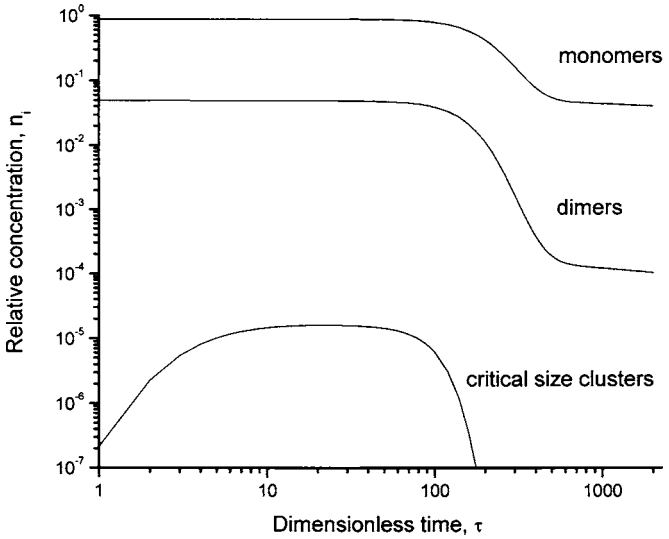

FIG. 5. Concentrations of monomers and dimers, and the critical size nuclei (n_c=11) vs time. Conditions as in example 2, Table I.

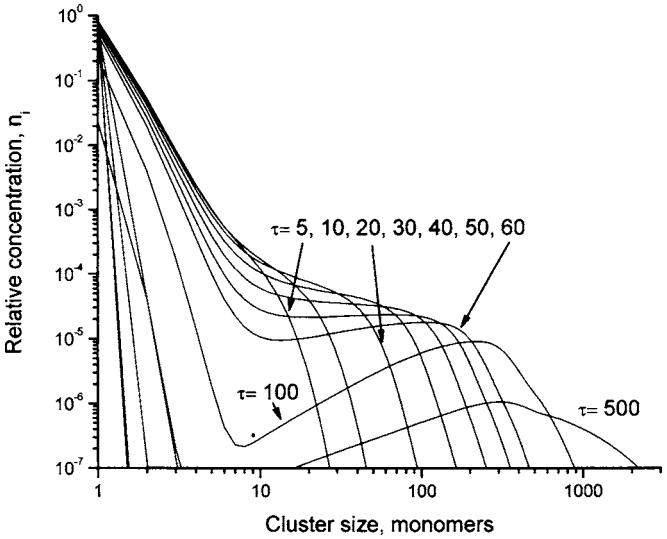

FIG. 7. Calculated dimensionless distribution functions of the cluster size. Conditions as in example 3, Table I.

Figure 6 illustrates the particle flux profiles that correspond to the steady state. The flux is not stable in time anymore, as it was in example 1. Also, it is not stable in the size domain, as the classical nucleation theory predicts. However, the steady-state nucleation rate obtained using the nucleation theory is close to the nucleation rate obtained in the numerical calculations. For example, at τ=20 the normalized monomer concentration is n_1=0.8715. Using Eq. (24) one obtains $J=6.12\times10^{-6}$, in agreement with the numerical modeling.

The dimensionless flux of 6×10^{-6} in this example corresponds to the nucleation rate of 1.9×10^{18} particle cm^{-3} s^{-1}. The experimental value for these conditions is $\sim(1-2)\times10^{16}$ particle cm^{-3} s^{-1}.[32] The difference can be partially attributed to the accommodation coefficient of water molecules on the surface of liquid water, $\sim$0.3.[41] Then, the residual difference is a factor of $\sim$20–50. To eliminate this discrepancy, the parameter Θ should be increased by about 8%.

From the experimental point of view, the most important result of this modeling is that the steady state exists in a narrow time interval, $10<\tau<80$. In the real time this corresponds to 0.6–5 μs. Under more extreme conditions which were achieved in the experiments with Laval nozzle, the validity of the steady-state assumption is even more problematic.

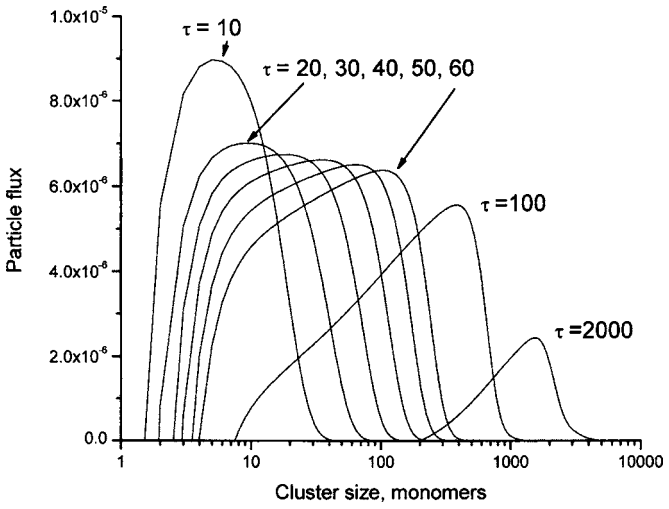

FIG. 6. The cluster flux profiles, J_k, at different dimensionless times, τ. Conditions as in example 2, Table I.

To illustrate this we performed numerical modeling with the parameters Θ=13.91 and S_0=120 (example 3, Table I). These parameters correspond to supersaturated water vapor at 210 K. The initial size of the critical nucleus is $n_{c,0}$ =7.28.

The time evolution of the dimensionless distribution function for this example is shown in Fig. 7. In sharp contrast with the previous examples, such as shown in Fig. 1, no steady-state distribution is ever established. At the very beginning of the process, at $\tau<5$, only small clusters are formed. After about τ=10, a "shoulder" on the distribution function begins to form. At this moment fast depletion of monomers occurs due to the condensation on large particles.

Detailed analysis of the consumption of monomers shows that there is a gap before the start of the condensation at τ=10–30. However, the flux profiles are not stable over this period. As it could be seen from Fig. 8, the flux monotonically decreases with time during this period. Surprisingly, the expression for the steady-state flux [Eq. (24)] at some moments still can predict the flux with a reasonable accuracy despite the absence of the steady state. For example, at τ=20, based on the current concentration of monomers at this time, n_1=0.797, the flux predicted by Eq. (24) is $J=0.97\times10^{-4}$. From the numerical calculations the peak value of the flux at this time is 1.27×10^{-4}. However, the absence of the steady state is important for the interpretation of the experimental data. For example, the formula for the homogeneous nucleation rate $J=N/\Delta t$, where N is the concentration of the clusters formed during time interval Δt, is not applicable anymore. Moreover, such a fortunate coincidence exists only at short times, the discrepancy increases with time and reaches orders of magnitude at later times (Fig. 8).

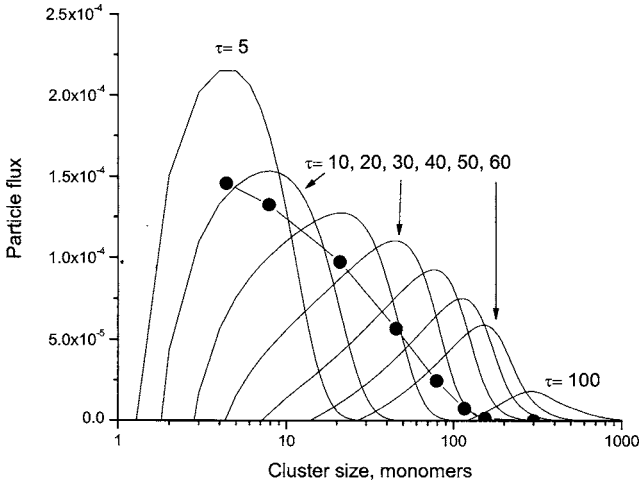

FIG. 8. The cluster flux profiles, J_k, at different dimensionless times, τ. Conditions as in example 3, Table I. The solid circles show the steady-state fluxes calculated using Eq. (24) based on the *current* monomer concentrations. The circles are placed under the maxima positions of the corresponding flux profiles. The steady-state flux calculated based on the initial monomer concentration is appreciably larger, $J_0=5.32\times10^{-4}$.

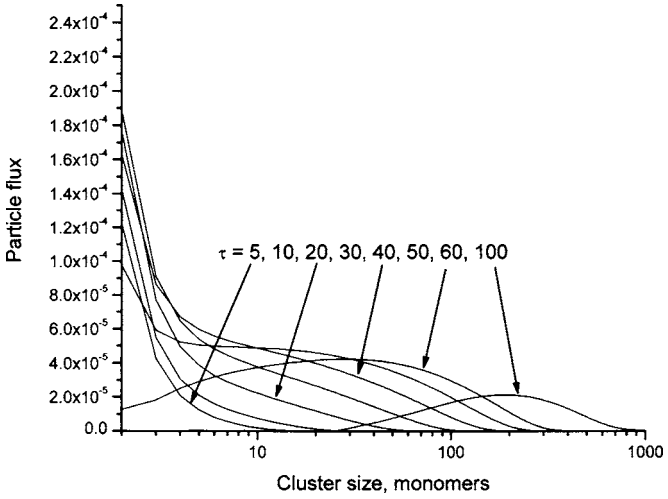

FIG. 9. The cluster flux profiles, J_k, at different dimensionless times, τ. Conditions as in example 3, Table I. The rate constant k_{11} is reduced 1000 times compared to the gas collision rate constant.

The dimensionless flux can be converted to the nucleation rate via multiplication of the dimensionless flux by the conversion factor, in this example by 1.1×10^{23} particle cm^{-3} s^{-1}. The nucleation rate obtained in this way is about 50 times larger than the experimental nucleation rates, $(1-2)\times10^{17}$ particle cm^{-3} s^{-1}.[32] The difference might again indicate the applicability of the Kelvin approximation to the thermodynamics of water clusters. However, as it is evident from the numerical results, the kinetic effects might play a role, too. Under the conditions when the steady state is not established, the individual rate constants starting from monomer-monomer, monomer-dimer, monomer-trimer, dimer-trimer, etc., might play a critical role. Under the steady state, the major contribution comes from the processes of monomer condensation/evaporation from clusters about the critical size, where (at relatively large critical nuclei) the assumption of the molecular condensation regime appears to be reasonable (may be corrected for the accommodation coefficient). However, when no steady state is established, and the rate constants of the very initial steps play a role, the assumption of the gas kinetic rate constants for these processes might lead to gross errors. The reaction of formation of water dimers is necessarily in the pressure falloff regime even at near atmospheric bath gas pressures.[43] The situation is much worse at the conditions of the Laval nozzle experiments,[32] where the bath gas pressure was only ~1–6 mbars. At pressures ~1 bar the difference of the third order rate constant and the second order gas kinetic rate constant is about 1000 times.[43] Rough estimates show that at the conditions of the Laval nozzle experiments one could expect deviations of the dimerization rate constant from the gas kinetic by three to four orders of magnitude. Smaller scale deviations could be expected for the subsequent reactions of monomers with dimers, etc. To at least evaluate the possible impact of these deviations, two additional series of calculations were performed using the model where the rate constant of the dimerization step was reduced by 10^3 and 10^6 times. The calculations show that the cluster size distribution functions and the rates of particle nucleation differ significantly. Figure 9 shows the particle flux profiles obtained with the dimensionless dimerization rate constant $\kappa_{11}=0.001$. The fluxes are about three times smaller compared to the case when $2\kappa_{11}=1$ (Fig. 8). For the dimerization rate constant reduced 10^6 times, Fig. 10, the fluxes are an order of magnitude smaller and are attained at an order of magnitude longer times. These examples illustrate the importance of the rates for the first steps of the nucleation process when the steady state is not really established.

The calculations based on the complete kinetic model show that at least in some of the experiments of water nucleation in the Laval nozzle the steady state might be not established. In such conditions the applicability of any version of the classical nucleation theory is not warranted, and direct numerical modeling is required.

The presented kinetic model (as well as the classical nucleation theory) has two dimensionless parameters, Θ and S_0. We performed a number of calculations varying these

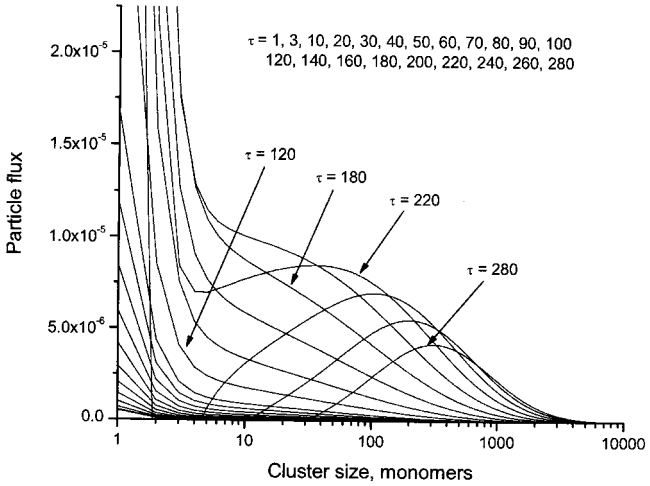

FIG. 10. The cluster flux profiles, J_k, at different dimensionless times, τ. Conditions as in example 3, Table I. The rate constant k_{11} is reduced 10^6 times compared to the gas collision rate constant.

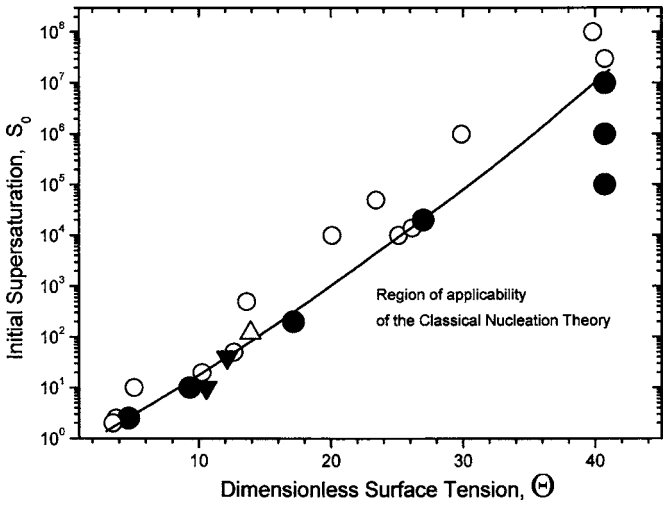

FIG. 11. The region of applicability of the steady-state assumption. The steady state is established in the region below the solid line (see text for the criteria). Open circles: model calculations where the particle flux does not stabilize at any time; solid circles: the particle flux profiles satisfy the criteria. Solid triangles: examples 1 and 2; open triangle: example 3 from Table I.

parameters over very wide ranges in order to determine the conditions when the steady-state assumption is applicable. The results of these calculations are presented in Fig. 11. The steady state is established in the lower section in Fig. 11. In other words, the lower region in Fig. 11 is the region of applicability of the steady-state assumption—one of the major assumptions of the classical theory of homogeneous nucleation. The criterion which was used to separate two regions was formulated based on the shape of the particle flux profiles. It is clear that the quantitative criterion can be chosen arbitrarily and should be determined based on the required accuracy. In Fig. 11, the criterion chosen was the flatness of the flux profile in the time domain (like in Fig. 2) within 20% over the time period from t_{min} to t_{max}, with at least $t_{max} > 3t_{min}$. It should be noted that the boundary outlined in Fig. 11 depends upon the chosen quantitative criterion, although the dependence is not too strong.

The results presented in Fig. 11 qualitatively confirm the generally accepted view that the classical theory of homogenous nucleation is applicable at small and moderate supersaturations, and cannot be used at large supersaturations. However, the position of the boundary depends on the dimensionless surface tension (parameter Θ). It should be emphasized that the boundary in Fig. 9 at different Θ corresponds to different sizes of the critical nucleus, $n_{c,0}$. The critical nucleus size can be obtained from Θ and S_0 using Eq. (18). For example, for Θ=5 the boundary corresponds to $n_{c,0}=50$, for Θ=10 the boundary corresponds to $n_{c,0}=15$, and for Θ=30 the boundary corresponds to $n_{c,0}=5.2$. If the dimensionless surface tension is large (high surface tension at low temperatures), the steady state can be achieved even with relatively small critical nucleus.

IMPACT OF THE THERMODYNAMIC INCONSISTENCY OF THE PARTIALLY REVERSIBLE KINETIC MODELS

The kinetic model, which is used as the foundation of the classical theory of nucleation, takes into account only the reactions of monomer condensation and evaporation.[4] The rates of evaporation are evaluated based on the condensation rates and the equilibrium concentrations of the corresponding clusters in saturated vapor. This kinetic model is thermodynamically consistent. The ratio of the forward and reverse rate constants is equal to the equilibrium constant (expressed in the concentration units); it is generally assumed that under some conditions this relationship holds for nonequilibrium states.[44] However, models that include only processes involving monomers cannot be used at the deep stages (e.g., the coagulation stage) of aerosol growth, when the excess concentration of monomers is already consumed and the processes of coagulation of larger clusters became important.

To address this issue, a modified kinetic model was introduced.[10] In addition to the monomer condensation/evaporation this model includes all reactions between clusters in the forward direction. The processes of evaporation of dimers, trimers, and larger clusters are neglected, which is justified by their low probability.

A closer look at the rate constants of the cluster evaporation shows that the rates of these reactions are not necessarily always negligible. For example, for Θ=10.57 and S_0 =10 (water at T=252 K, see example 1 in Table I) the rate constants of the dimer evaporation from clusters below the critical size are only from 1.5 to 13 times smaller than the rate constants for the evaporation of monomers (Table II). What is even more important is that this kinetic model is thermodynamically inconsistent. Taking into account only forward reactions and neglecting the corresponding reverse reactions of dimers, trimers, etc., while for the processes involving monomers using both forward and reverse reactions, is in conflict with the principle of detailed balance. When the system is at equilibrium or close to equilibrium such a model predicts kinetic "cycles" which are thermodynamically forbidden. An example of such a cycle is a sequence of the coagulation reaction of a cluster with a dimer followed by subsequent evaporation of two monomers.

Reliable analytical evaluation of the errors in the distribution functions caused by neglecting the reactions of cluster evaporation is difficult. Therefore, we performed numerical model calculations in order to evaluate these errors. The calculations were performed with the parameters of example 1,

TABLE II. Dimensionless rate constants for the reactions of monomer and dimer evaporation, $P_{i+1} \rightarrow P_i + P_1$ and $P_{i+2} \rightarrow P_i + P_2$, calculated using expressions 16 and 17. Θ=10.57, S_0=10.

Process	i=3	i=6	i=10	i=29	i=50	i=200
$P_{i+1} \rightarrow P_i + P_1$	10.3	6.03	4.39	2.88	2.62	4.05
$P_{i+2} \rightarrow P_i + P_2$	6.22	1.90	0.85	0.22	0.133	0.064

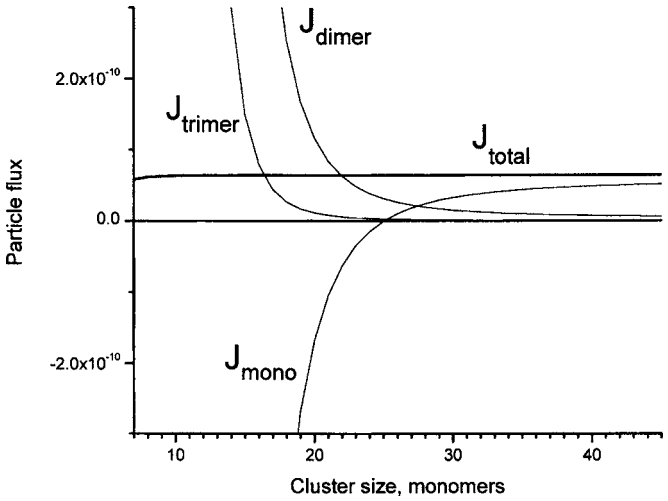

FIG. 12. The cluster flux profile, J_k, at the dimensionless time $\tau=300$ obtained using the kinetic model with zero rate constants of dimers, trimers, etc., evaporation. Conditions are as in example 1, Table I.

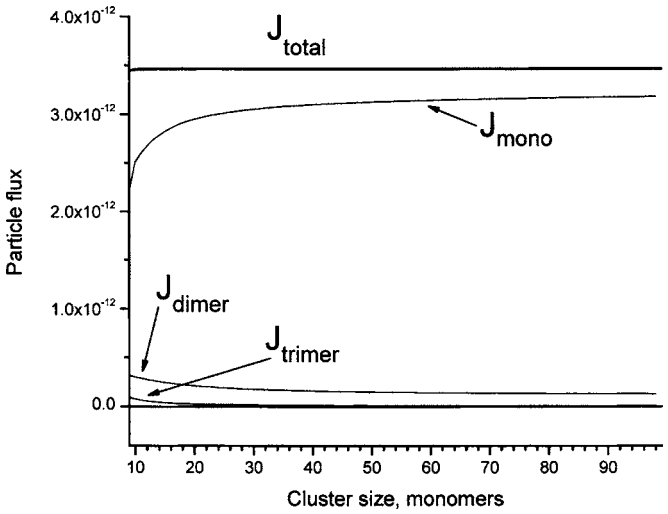

FIG. 13. The cluster flux profile, J_k, and the components of these fluxes. Complete kinetic model. Dimensionless time $\tau=300$. Conditions are as in example 1, Table I.

Table I (water at 252 K). The rate constants for all reverse reactions except for the monomer evaporation were set to zero. The comparison of the steady-state distribution functions obtained in these calculations with the steady-state distribution functions for the complete model (Fig. 1) shows the error of about one order of magnitude. The dimensionless steady-state particle flux is larger by about one order of magnitude as well, 6.4×10^{-11} vs 3.4×10^{-12}. Figure 12 shows the particle flux profile for $\tau=300$ and the contributions to the flux. The steady state obtained in the calculations is characterized by the particle flux that is stable in the time and size domains. In Fig. 12 it is labeled as J_{total}. The total particle flux could be divided to flux caused by the monomer condensation/evaporation reactions, J_{mono}, the dimer reactions, J_{dimer}, the trimer reactions, J_{trimer}, etc. The monomer component could be calculated using

$$J_{\text{mono}} = \kappa_{1,i} n_1 n_i - \kappa'_{1,i} n_{i+1}. \tag{26}$$

The dimer contribution is

$$J_{\text{dimer}} = \kappa_{2,i} n_2 n_i - \kappa'_{2,i} n_{i+2}. \tag{27}$$

The trimer and other contributions to the flux are calculated similarly.

The contributions of monomers, dimers, and trimers to the total flux calculated based on Eqs. (26) and (27) are presented in Fig. 12. It could be seen that for clusters smaller than 24 monomers, the monomer component of the flux is negative in contrast to the other components. Different signs of the fluxes make the existence of the "kinetic cycles" in the steady state evident. The large positive flux caused by dimer and trimer condensation is compensated by a large negative flux of monomer flux (mainly evaporation of monomers). It is apparent that the kinetic cycles in this thermodynamically inconsistent kinetic model lead to large errors in the steady-state nucleation rates.

It should be stressed that the demonstration of the magnitude of the impact of the "kinetic cycles" in Fig. 12 is not based upon the rate constants for the dimer and trimer evaporation obtained using the Kelvin model. These rate constants are set to zero. Only the rate constants for monomer evaporation, calculated using the Kelvin model, were used.

The contributions to the steady-state particle flux obtained using the complete, thermodynamically consistent kinetic model are shown in Fig. 13. In contrast with Fig. 12, all the components of the particle flux are now positive. The main contribution to the nucleation rate is due to the reactions of monomers. As it should be, no kinetic cycles are observed in the steady state obtained by thermodynamically consistent kinetic model.

In the considered example the error in the nucleation rate caused by the thermodynamic inconsistency of the kinetic model is about one order of magnitude. Under different conditions the errors could be much larger. For lower supersaturation ($\Theta=4.66$ and $S_0=4$) the error in the nucleation rate obtained with the inconsistent kinetic model was about three orders of magnitude. These examples show that the thermodynamic inconsistency might lead to large errors, and that such models should be used with caution.

Numerical calculations described above are based on the Kelvin model, applicability of which for small clusters is questionable at best. One can argue that the impact of such inconsistencies might be not as significant if more realistic thermodynamics is used. However, the comparison of the recent theoretical calculations[29] and the experimental data[45] for water clusters with the Kelvin model shows that the Kelvin model can be used for reliable estimates. Figure 14 shows the standard Gibbs energy of formation of water clusters from monomers at 298 K based on the discrete Kelvin model, as well as the results of quantum chemical calculations[29] and the experimental data for water dimers.[45] It is apparent that the predictions of the Kelvin model are in good agreement with the calculations and the experimental data. It should be noted, however, that there are theoretical calculations that do not agree so well with the Kelvin model. The Monte Carlo simulations of water clusters consisting of 2–10 water molecules at 243 K resulted in the reversible work of cluster formation ~10%–30% larger than predicted by the Kelvin model.[46]

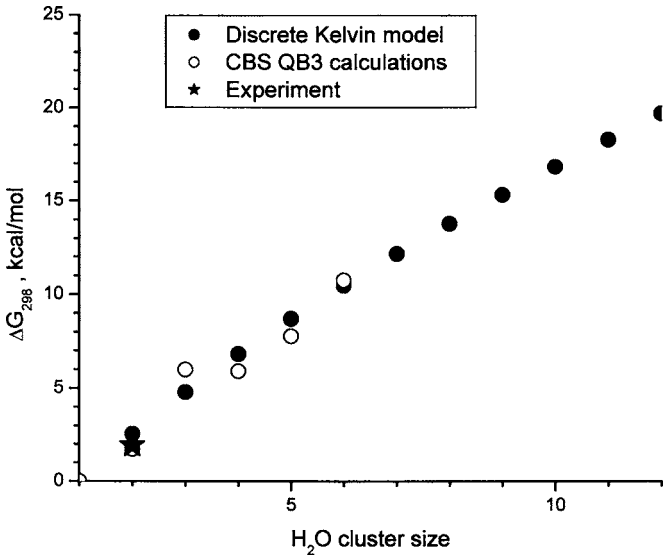

FIG. 14. The standard Gibbs energy of formation of the water clusters from monomers. Open circles: CBS-QB3 calculation (Ref. 29) filled circles: the discrete Kelvin model; stars: the experiment (Ref. 45).

CONCLUSIONS

In this work, a complete thermodynamically consistent elementary reaction kinetic model of particle nucleation and growth from supersaturated vapor was developed and numerically evaluated. The model treats all processes recognized in the aerosol science (such as nucleation, condensation, evaporation, agglomeration/coagulation, etc.) as reversible elementary reactions. It includes all possible forward reactions (i.e., of monomers, dimers, trimers, etc.) together with the thermodynamically consistent reverse processes.

Numerical calculations were performed under the assumptions accepted in the classical nucleation theory (the surface tension approximation for the particle thermodynamics and simple collision theory for the forward processes) for several sets of parameters consistent with the existing experiments on water vapor condensation as well as several model sets of parameters including very extreme as encountered in Laval nozzle experiments and nanoparticle formation by rapid expansion of supercritical solutions. It was shown that the main assumption of the classical nucleation theory—the steady-state approximation—breaks already at the supersaturations about 100 comparable with the supersaturations achievable in the Laval nozzle experiments. The point is made that under the conditions when no steady state is achieved the specific rate constants of the very initial stages of nucleation (dimerization, trimerization, etc.) become important, and evaluation of these rate constants as gas kinetic might lead to gross errors. This is especially important to water as this is a small molecule forming a relatively weakly bound dimers, so that the assumption of the gas kinetic rate constant for the dimerization might be in several orders of magnitude error under the typical experimental conditions. The impact of the thermodynamic inconsistency of the previously developed partially reversible kinetic models was assessed. At some experimental conditions typical for water nucleation, the error in the nucleation rate introduced by the thermodynamic inconsistency could be about an order of magnitude.

ACKNOWLEDGMENTS

Partial support for this work was provided by the US EPA Center on Airborne Organic (MIT/NJIT/CALTECH), Grant No. R824970-01-0, and by the US Army ARDEC under Contract No. DAAE30-02-C-1140, funded via the Picatinny Arsenal Nanovalley program.

APPENDIX A: CLUSTER FORMATION/DISSOCIATION REACTIONS IN TERMS OF CHEMICAL THERMODYNAMICS

The purpose of this section is to formulate the thermodynamic properties of the cluster formation/dissociation reactions using the approach and the definitions of chemical thermodynamics. Since the main purpose of the paper is to describe the process of particle nucleation and growth in terms of chemical kinetics of the gas-phase reactions, the thermodynamics of these reactions is also treated on the bases of the gas-phase reactions.

We treat clusters of all sizes as the gas-phase components. The bulk liquid (with the infinite radius of curvature) is treated as the liquid phase. For the gas-phase species [such as clusters $P_n(g)$] the standard state is defined as the hypothetical state of *ideal gas* of pure clusters P_n at the standard pressure p^Θ. It should be noted that the value of the standard pressure (currently accepted $p^\Theta = 1$ bar) is not important for the discussion below. For the bulk liquid, the standard state is defined as pure *real liquid* at pressure p^Θ. Thus, for the evaporation process from the liquid phase into a gas of monomers, the standard Gibbs energy of vaporization, $\Delta G^\Theta_{\mathrm{vap},1}$, refers to the process

$$P(l) \Leftrightarrow P_1(g), \quad \Delta G^\Theta_{\mathrm{vap},1}. \tag{A1}$$

Under the assumption of ideal gas of vapor Eq. (A1) implies

$$p_1^*/p^\Theta = \exp(-\Delta G^\Theta_{\mathrm{vap},1}/RT), \tag{A2}$$

where p_1^* is the equilibrium partial vapor pressure of monomers above a flat liquid surface.

In addition to Eq. (A1), we will use processes involving clusters of all sizes that are treated as reactions of gas-phase species,

$$P_n(g) + P_m(g) \rightleftharpoons P_{n+m}(g), \quad \Delta G^\Theta_{n,m}, \tag{A3}$$

$$P_n(g) + P_1(g) \rightleftharpoons P_{n+1}(g), \quad \Delta G^\Theta_{n,1}, \tag{A4}$$

$$nP_1(g) \rightleftharpoons P_n(g), \quad \Delta G^\Theta_{\mathrm{cond},n}, \tag{A5}$$

where the standard Gibbs energy is defined according to the definitions accepted in chemical thermodynamics. For example, for reaction (A3), $\Delta G^\Theta_{n,m}$ is the difference of the Gibbs energy of 1 mole of clusters P_{n+m} in a hypothetical state of ideal gas at pressure p^Θ and the Gibbs energy of unmixed 1 mole of clusters P_n and 1 mole of clusters P_m in the hypothetical ideal gas states both at pressure p^Θ.

Let us first discuss the process of monomer condensation/evaporation [Eq. (A4)]. The equilibrium constant for this reaction is calculated based on the standard Gibbs energy of reaction (A4), $\Delta G^{\Theta}_{n,1}$.

To derive the standard Gibbs energy of reaction (A4), the "surface tension model" is invoked. The model is based on the Kelvin formula (A6) for the equilibrium (unstable) vapor pressure above a spherical surface,

$$p = p^* \exp\left(\frac{2\gamma V_{m,l}}{rRT}\right). \tag{A6}$$

In this expression, p is the (unstable) equilibrium vapor pressure above a spherical particle with the radius r, p^* is the stable equilibrium vapor pressure above a flat surface, γ is the surface tension between the liquid and vapor, and $V_{m,1}$ is the molar volume of monomers in the liquid phase. Expression (A6) is valid assuming that dimers, trimers, etc., contribute negligible in the equilibrium vapor pressure, that all components obey the ideal gas law, and that the aerosol particles are incompressible, and neglecting the molar volume of liquid in comparison with the molar volume of vapor. Based on the fact that Eq. (A6) describes equilibrium (although unstable) one can argue that the equilibrium concentrations of n_c-mers and (n_c+1)-mers should be equal (the discrete analog of the extremum condition),

$$N_{n_c} = N_{n_c+1}, \tag{A7}$$

where n_c is the size of the cluster which is in equilibrium (unstable) with the vapor at a given partial vapor pressure of monomers, i.e., the critical nucleus size. The same results can be also derived based on the fact that the Gibbs energy of condensation of n-mers from monomers has an extremum (maximum) at the critical nucleus size. Equating the rates of the forward and the reverse processes in Eq. (A4) for $n=n_c$ (equilibrium), one derives

$$k_{n_c,1} N_{n_c} N_1 = N_{n_c+1} k'_{n_c,1}. \tag{A8}$$

The thermodynamic equilibrium constant for reaction (A4) is defined as (ideal gas behavior for all components is assumed)

$$K_{n,1} = \frac{P_{n+1}/p^{\theta}}{(p_n/p^{\theta})(p_1/p^{\theta})} = \frac{p^{\theta} N_A}{RT} \frac{N_{n+1}}{N_n N_1}, \tag{A9}$$

where $p^{\Theta}=1$ bar is the standard pressure, N_A is Avogadro's number, and all partial pressures and concentrations refer to the equilibrium conditions.

The standard Gibbs energy of reaction (A4) is then

$$\Delta G^{\Theta}_{n,1} = -RT \ln(K_{n,1}). \tag{A10}$$

For $n=n_c$, using $p_{n_c}=p_{n_c+1}$ [Eq. (A7)], Eq. (A9) can be rearranged as

$$K_{n_c,1} = \frac{1}{(p_1/p^{\theta})} = \frac{1}{(p_1/p_1^*)(p_1^*/p^{\theta})}. \tag{A11}$$

The ratio p_1^*/p^{Θ} is controlled by the standard Gibbs energy of vaporization of monomers, i.e., process (A1). The ratio p_1/p_1^* is given by the Kelvin formula which is extended to the clusters of any size, including monomers. Finally, combining Eqs. (A2), (A6), (A7), and (A10) we obtain the standard Gibbs energy of reaction (A4),

$$\Delta G^{\Theta}_{n,1} = -\Delta G^{\Theta}_{\mathrm{vap},1} + 2\gamma V_{m,l}/r_{n+1}, \tag{A12}$$

where r_{n+1} is the radius of a cluster containing $(n+1)$ monomers. In Eq. (A12) n_c is replaced with an arbitrary n, since the critical nucleus can be made of any size by varying the partial pressure; therefore, Eq. (A12) is applicable to any cluster size (of course under the extension of the surface tension model down to the monomer size).

Applying sequential attachment of monomers, for the process of condensation of a n-mer from n monomers in the gas phase [Eq. (A5)] one derives

$$\Delta G^{\theta}_{\mathrm{cond},n} = -(n-1)\Delta G^{\theta}_{\mathrm{vap},1} + \sum_{i=2}^{n} \frac{2\gamma V_{m,l}}{r_i}. \tag{A13}$$

Using the radius of the monomer r_1,

$$r_i = r_1 i^{1/3}, \tag{A14}$$

expression (A13) is rewritten as

$$\Delta G^{\theta}_{\mathrm{cond},n} = -(n-1)\Delta G^{\theta}_{\mathrm{vap},1} + \frac{2\gamma V_{m,l}}{r_1} \sum_{i=2}^{n} \frac{1}{i^{1/3}}. \tag{A15}$$

Then the standard Gibbs energy for an arbitrary process described by the stoichiometric equation [Eq. (A3)] is

$$\begin{aligned}\Delta G^{\theta}_{n,m} &= \Delta G^{\theta}_{\mathrm{cond},n+m} - \Delta G^{\theta}_{\mathrm{cond},n} - \Delta G^{\theta}_{\mathrm{cond},m} \\ &= -\Delta G^{\theta}_{\mathrm{vap},1} + \frac{2\gamma V_{m,l}}{r_1}\left(\sum_{i=2}^{n+m} \frac{1}{i^{1/3}} - \sum_{i=2}^{n} \frac{1}{i^{1/3}} - \sum_{i=2}^{m} \frac{1}{i^{1/3}}\right).\end{aligned} \tag{A16}$$

Incorporating the standard notations for the dimensionless surface energy of the monomers,[26]

$$\Theta = \frac{4\pi r_1^2 \gamma}{k_B T} = \frac{\pi^{1/3}(6V_1)^{2/3}}{k_B T}. \tag{A17}$$

Here V_1 is the volume of the monomer. Both V_1 and the radius r_1 are *defined* as

$$V_1 = V_{m,l}/N_A = (4\pi/3) r_1^3. \tag{A18}$$

Equation (A16) becomes

$$\Delta G^{\theta}_{n,m} = -\Delta G^{\theta}_{\mathrm{vap},1} + RT \frac{2\Theta}{3}\left(\sum_{i=2}^{n+m} \frac{1}{i^{1/3}} - \sum_{i=2}^{n} \frac{1}{i^{1/3}} - \sum_{i=2}^{m} \frac{1}{i^{1/3}}\right). \tag{A19}$$

Finally, the reverse rate constants for reaction (1) are calculated based on the principle of detailed balance,

$$k'_{nm} = \left(\frac{p^{\theta}N_A}{RT}\right)\left(\frac{k_{nm}}{K_{nm}}\right)$$
$$= k_{nm}\left(\frac{p^{\theta}N_A}{RT}\right)\exp\left(\frac{\Delta G^{\theta}_{n,m}}{RT}\right)$$
$$= k_{nm}\left(\frac{p^{\theta}N_A}{RT}\right)\exp\left(-\frac{\Delta G^{\theta}_{\mathrm{vap},1}}{RT}\right)\exp\left(\frac{2\Theta}{3}\left(\sum_{i=2}^{n+m}\frac{1}{i^{1/3}} - \sum_{i=2}^{n}\frac{1}{i^{1/3}} - \sum_{i=2}^{m}\frac{1}{i^{1/3}}\right)\right)$$
$$= k_{nm}\left(\frac{p^{\theta}N_A}{RT}\right)\left(\frac{p_1^*}{p^{\theta}}\right)\exp\left(\frac{2\Theta}{3}\left(\sum_{i=2}^{n+m}\frac{1}{i^{1/3}} - \sum_{i=2}^{n}\frac{1}{i^{1/3}} - \sum_{i=2}^{m}\frac{1}{i^{1/3}}\right)\right). \quad \text{(A20)}$$

Introducing the current supersaturation, S, current number density of the monomers, N_1, and the equilibrium number density of monomers above a flat surface, N_1^*,

$$S = \frac{N_1}{N_1^*} \approx \frac{p_1}{p_1^*}. \quad \text{(A21)}$$

Equation (A20) transforms to

$$k'_{nm} = k_{nm}N_1\left(\frac{1}{S}\right)\exp\left(\frac{2\Theta}{3}\left(\sum_{i=2}^{n+m}\frac{1}{i^{1/3}} - \sum_{i=2}^{n}\frac{1}{i^{1/3}} - \sum_{i=2}^{m}\frac{1}{i^{1/3}}\right)\right), \quad \text{(A22)}$$

which leads to the dimensionless equation [Eq. (17)] in the main text of the paper.

APPENDIX B: SECTIONING (BINNING) APPROACH FOR THE REVERSIBLE MODEL OF CLUSTER NUCLEATION AND GROWTH

In this appendix, the sectioning (binning) approach as well as the main principles of the computer code are summarized.

A section (bin) is defined as an interval for the cluster size, in terms of the number of monomers. The notation for the sections is S_α where $\alpha = 1,2,3,4,\ldots$. A set of sections is characterized by a small parameter ε. Let b_α be the size of the smallest cluster in section S_α, then the width W_α of the section S_α is calculated as

$$W_\alpha \leqslant 1 + \varepsilon b_\alpha, \quad \text{(B1)}$$

where the result should be rounded off to the closest integer value. For example, for $\varepsilon = 0.01$ the width of the first 99 sections is 1, the next 50 sections has the width 2, and so on. The first 99 sections form the discrete region, but we treat this region in the same manner as all other sections. The differential equations for the sections are written in such a way that if a section has the unit width, then the differential equation for the section is equivalent to the original discrete equation.

Let us consider a collision of clusters from sections S_α and S_β. The products of such reaction can belong to several sections. Let S_γ be the lowest section of the products of this reaction. The closer examination of the section system [Eq. (B1)] shows that the products could belong maximum to three sections,

$$S_\alpha + S_\beta \rightarrow S_\gamma, S_{\gamma+1}, S_{\gamma+2}. \quad \text{(B2)}$$

Let $\xi^{(0)}_{\alpha,\beta}$ be the number of events, when the product belongs to section S_γ, $\xi^{(1)}_{\alpha,\beta}$ the number of events when the product belongs to section $S_{\gamma+1}$, and $\xi^{(2)}_{\alpha,\beta}$ the number of events when the product belongs to section $S_{\gamma+2}$. Then

$$\xi^{(0)}_{\alpha,\beta} = \sum_{i\in S_\alpha}\sum_{j\in S_\beta}\sum_{k\in S_\gamma}\delta(i+j-k), \quad \text{(B3)}$$

where $\delta(n)$ is the discrete delta function: $\delta(0)=1$, $\delta(n)=0$ if $n \neq 0$. The $\xi^{(1)}_{\alpha,\beta}$ and $\xi^{(2)}_{\alpha,\beta}$ could be calculated in a similar way,

$$\xi^{(1)}_{\alpha,\beta} = \sum_{i\in S_\alpha}\sum_{j\in S_\beta}\sum_{k\in S_{\gamma+1}}\delta(i+j-k), \quad \text{(B4)}$$

$$\xi^{(2)}_{\alpha,\beta} = \sum_{i\in S_\alpha}\sum_{j\in S_\beta}\sum_{k\in S_{\gamma+2}}\delta(i+j-k). \quad \text{(B5)}$$

When calculating $\xi^{(0)}_{\alpha,\beta}$, the code simultaneously calculates the average clusters sizes $\langle i\rangle$ and $\langle j\rangle$ in the case when the products belong to section S_γ,

$$\langle i\rangle^{(0)}_{\alpha,\beta} = \frac{1}{\xi^{(0)}_{\alpha,\beta}}\sum_{i\in S_\alpha}\sum_{j\in S_\beta}\sum_{k\in S_\gamma} i\delta(i+j-k),$$
$$\langle j\rangle^{(0)}_{\alpha,\beta} = \frac{1}{\xi^{(0)}_{\alpha,\beta}}\sum_{i\in S_\alpha}\sum_{j\in S_\beta}\sum_{k\in S_\gamma} j\delta(i+j-k). \quad \text{(B6)}$$

These average cluster sizes are used to calculate the average rate constant $\Re^{(0)}_{\alpha,\beta}$ for the process $S_\alpha + S_\beta \rightarrow S_\gamma$ in the forward direction,

$$\Re^{(0)}_{\alpha,\beta} = \frac{1}{4\sqrt{2}}(\langle i\rangle^{1/3} + \langle j\rangle^{1/3})^2(1/\langle i\rangle + 1/\langle j\rangle)^{1/2} \quad \text{(B7)}$$

and the average rate constant in the reverse direction,

$$\Re'^{(0)}_{\alpha,\beta} = \Re^{(0)}_{\alpha,\beta}\exp\left(\frac{2\Theta}{3}\left(\sum_{k=2}^{\langle i\rangle+\langle j\rangle}k^{-1/3} - \sum_{k=2}^{\langle i\rangle}k^{-1/3} - \sum_{k=2}^{\langle j\rangle}k^{-1/3}\right)\right)\Big/ S_0. \quad \text{(B8)}$$

In the case when the product belongs to section $S_{\gamma+1}$, the average cluster sizes are calculated in a similar way,

$$\langle i\rangle^{(1)}_{\alpha,\beta} = \frac{1}{\xi^{(1)}_{\alpha,\beta}}\sum_{i\in S_\alpha}\sum_{j\in S_\beta}\sum_{k\in S_{\gamma+1}} i\delta(i+j-k), \quad \text{(B9)}$$

$$\langle j\rangle^{(1)}_{\alpha,\beta} = \frac{1}{\xi^{(1)}_{\alpha,\beta}}\sum_{i\in S_\alpha}\sum_{j\in S_\beta}\sum_{k\in S_{\gamma+1}} j\delta(i+j-k). \quad \text{(B10)}$$

These average cluster sizes are for the calculations of the average rate constants $\Re^{(1)}_{\alpha,\beta}$ and $\Re'^{(1)}_{\alpha,\beta}$. Similarly, the average rate constants $\Re^{(2)}_{\alpha,\beta}$ and $\Re'^{(2)}_{\alpha,\beta}$ are calculated for the processes leading to the products that belong to section $S_{\gamma+2}$.

Consequently, a collision of clusters from sections α and β is described by the following parameters:

$$\gamma, \quad \xi^{(0)}_{\alpha,\beta}, \quad \xi^{(1)}_{\alpha,\beta}, \quad \xi^{(2)}_{\alpha,\beta}, \quad \Re^{(0)}_{\alpha,\beta}, \quad \Re'^{(0)}_{\alpha,\beta},$$
$$\Re^{(1)}_{\alpha,\beta}, \quad \Re'^{(1)}_{\alpha,\beta}, \quad \Re^{(2)}_{\alpha,\beta}, \quad \Re'^{(2)}_{\alpha,\beta}. \tag{B11}$$

Before the start of numerical integrations of the set of differential equations, the code calculates these parameters and stores in the memory. The data structure is then 10 numbers for each combination of sections. These precalculated numbers are then used for calculations of the right hand sides of the differential equations.

We used the differential equation in terms of the section populations,

$$B_\alpha = \sum_{i \in S_\alpha} n_i. \tag{B12}$$

A reaction between clusters from sections S_α and S_β might change the populations of the five following sections: S_α, S_β, S_γ, $S_{\gamma+1}$, and $S_{\gamma+2}$. The correspondent terms in the right hand sides of differential equations are

$$\frac{dB_\alpha}{d\tau} = \cdots \frac{\xi^{(0)}_{\alpha,\beta}\Re^{(0)}_{\alpha,\beta} + \xi^{(1)}_{\alpha,\beta}\Re^{(1)}_{\alpha,\beta} + \xi^{(2)}_{\alpha,\beta}\Re^{(2)}_{\alpha,\beta}}{\xi^{(0)}_{\alpha,\beta} + \xi^{(1)}_{\alpha,\beta} + \xi^{(2)}_{\alpha,\beta}} B_\alpha B_\beta \cdots$$
$$+ \xi^{(0)}_{\alpha,\beta}\Re'^{(0)}_{\alpha,\beta} B_\gamma + \xi^{(1)}_{\alpha,\beta}\Re'^{(1)}_{\alpha,\beta} B_{\gamma+1}$$
$$+ \xi^{(2)}_{\alpha,\beta}\Re'^{(2)}_{\alpha,\beta} B_{\gamma+2} \cdots, \tag{B13}$$

$$\frac{dB_\beta}{d\tau} = \cdots \frac{\xi^{(0)}_{\alpha,\beta}\Re^{(0)}_{\alpha,\beta} + \xi^{(1)}_{\alpha,\beta}\Re^{(1)}_{\alpha,\beta} + \xi^{(2)}_{\alpha,\beta}\Re'^{(2)}_{\alpha,\beta}}{\xi^{(0)}_{\alpha,\beta} + \xi^{(1)}_{\alpha,\beta} + \xi^{(2)}_{\alpha,\beta}} B_\alpha B_\beta \cdots$$
$$+ \xi^{(0)}_{\alpha,\beta}\Re'^{(0)}_{\alpha,\beta} B_\gamma + \xi^{(1)}_{\alpha,\beta}\Re'^{(1)}_{\alpha,\beta} B_{\gamma+1}$$
$$+ \xi^{(2)}_{\alpha,\beta}\Re'^{(2)}_{\alpha,\beta} B_{\gamma+2} \cdots, \tag{B14}$$

$$\frac{dB_\gamma}{d\tau} = \cdots + \frac{\xi^{(0)}_{\alpha,\beta}}{\xi^{(0)}_{\alpha,\beta} + \xi^{(1)}_{\alpha,\beta} + \xi^{(2)}_{\alpha,\beta}} \Re'^{(0)}_{\alpha,\beta} B_\alpha B_\beta \cdots$$
$$- \frac{\xi^{(0)}_{\alpha,\beta}}{W_\gamma} \Re'^{(0)}_{\alpha,\beta} B_\gamma \cdots, \tag{B15}$$

$$\frac{dB_{\gamma+1}}{d\tau} = \cdots + \frac{\xi^{(1)}_{\alpha,\beta}}{\xi^{(0)}_{\alpha,\beta} + \xi^{(1)}_{\alpha,\beta} + \xi^{(2)}_{\alpha,\beta}} \Re^{(1)}_{\alpha,\beta} B_\alpha B_\beta \cdots$$
$$- \frac{\xi^{(1)}_{\alpha,\beta}}{W_{\gamma+1}} \Re'^{(1)}_{\alpha,\beta} B_{\gamma+1} \cdots, \tag{B16}$$

$$\frac{dB_{\gamma+2}}{d\tau} = \cdots + \frac{\xi^{(2)}_{\alpha,\beta}}{\xi^{(0)}_{\alpha,\beta} + \xi^{(1)}_{\alpha,\beta} + \xi^{(2)}_{\alpha,\beta}} \Re^{(2)}_{\alpha,\beta} B_\alpha B_\beta \cdots$$
$$- \frac{\xi^{(2)}_{\alpha,\beta}}{W_{\gamma+2}} \Re'^{(2)}_{\alpha,\beta} B_{\gamma+2} \cdots. \tag{B17}$$

A cycle of calculations of the right hand sides of the set of differential equations consists of sequential processing of all the combinations S_α and S_β. For each combination S_α and S_β the terms (B13)–(B17) are calculated and the results are stored.

[1] R. Becker and W. Doring, Ann. Phys. **24**, 719 (1935).
[2] J. Zeldovich, J. Exp. Theor. Phys. **12**, 525 (1942).
[3] J. Frenkel, *Kinetic Theory of Liquids* (Dover, New York, 1955).
[4] J. Katz and M. Donohue, Adv. Chem. Phys. **40**, 137 (1979).
[5] W. G. Courtney, J. Chem. Phys. **36**, 2009 (1961).
[6] A. A. Mazlovskii, Kolloidnyi Zhurnal **32**, 238 (1970).
[7] P. H. McMurry and S. K. Friedlander, Atmos. Environ. **13**, 1635 (1979); P. H. McMurry, J. Colloid Interface Sci. **78**, 513 (1980); **93**, 72 (1983).
[8] F. Gelbard and J. H. Seinfeld, J. Colloid Interface Sci. **68**, 363 (1979).
[9] S. K. Friedlander, Ann. N.Y. Acad. Sci. **404**, 354 (1983).
[10] S. K. Friedlander, *Smoke, Dust and Haze: Fundamentals of Aerosol Behavior* (Wiley-Interscience, New York, 1977).
[11] S. L. Girshick and C. P. Chiu, J. Aerosol Sci. **21**, 641 (1990).
[12] P. P. Bolsaitis, J. F. McCarthy, G. Mohiuddin, and J. F. Elliott, Aerosol Sci. Technol. **6**, 225 (1987).
[13] A. A. Onischuk, A. I. Levykin, V. P. Strunin, M. A. Ushakova, R. I. Samojlova, K. K. Sabelfeld, and V. N. Panfilov, J. Aerosol Sci. **31**, 879 (2000).
[14] S. N. Dubtsov, A. I. Levykin, and K. K. Sabelfeld, J. Aerosol Sci. **31**, 509 (2000).
[15] S. L. Girshick, C. P. Chiu, and P. H. McMurry, Aerosol Sci. Technol. **13**, 465 (1990).
[16] N. P. Rao and P. H. McMurry, Aerosol Sci. Technol. **11**, 120 (1989).
[17] K. P. Koutzenogii, A. I. Levykin, and K. K. Sabelfeld, J. Aerosol Sci. **27**, 665 (1996).
[18] S. E. Pratsinis, T. T. Kodas, M. P. Dudukovic, and S. K. Friedlander, Ind. Eng. Chem. Process Des. Dev. **25**, 634 (1986).
[19] J. J. Wu and R. C. Flagan, J. Colloid Interface Sci. **123**, 339 (1988).
[20] C. Y. Wu and P. Biwas, Aerosol Sci. Technol. **29**, 359 (1998).
[21] D. T. Wu, J. Chem. Phys. **97**, 2644 (1992).
[22] J. L. Katz, H. Saltsburg, and H. Reiss, J. Colloid Interface Sci. **21**, 560 (1966).
[23] H. Arstila, J. Chem. Phys. **107**, 3196 (1997).
[24] J. Frenkel, J. Chem. Phys. **7**, 538 (1939).
[25] V. A. Shneidman and M. C. Weinberg, J. Chem. Phys. **97**, 3629 (1992).
[26] S. L. Girshick and C. P. Chiu, J. Chem. Phys. **93**, 1273 (1990).
[27] J. L. Katz, Pure Appl. Chem. **64**, 1661 (1992).
[28] G. Wilemski, J. Chem. Phys. **103**, 1119 (1995).
[29] M. E. Dunn, E. K. Pokon, and G. C. Shields, J. Am. Chem. Soc. **126**, 2647 (2004).
[30] G. K. Schenter, S. M. Kathmann, and B. C. Garrett, Phys. Rev. Lett. **82**, 3484 (1999).
[31] V. Stepanov, I. B. Elkina, X. Zhang, and L. N. Krasnoperov, Propellants, Explos., Pyrotech. **30**, 178 (2005).
[32] Y. J. Kim, B. E. Wyslouzil, G. Wilemski, J. Wolk, and R. Strey, J. Phys. Chem. A **108**, 4365 (2004).
[33] S. N. Dubtsov, E. N. Chesnokov, and L. N. Krasnoperov, Atmos. Oceanic Opt. **15**, 445 (2002).
[34] F. Gelbard and J. H. Seinfeld, J. Colloid Interface Sci. **78**, 485 (1980).
[35] J. R. Brock, P. J. Kuhn, and D. Zehavi, J. Aerosol Sci. **17**, 11 (1986).
[36] P. Middleton and J. R. Brock, J. Colloid Interface Sci. **54**, 249 (1976).
[37] J. D. Landgrebe and S. E. Pratsinis, J. Colloid Interface Sci. **139**, 63 (1990).
[38] W. H. Press, S. A. Teukolsky, W. T. Vetterling, and B. P. Flannery, *Numerical Recipes in C: The Art of Scientific Computing*, 2nd ed. (Cambridge University Press, New York, 2002).
[39] J. Wolk and R. Strey, J. Phys. Chem. B **105**, 11683 (2001).
[40] J. L. Katz and H. Wiedersich, J. Colloid Interface Sci. **61**, 351 (1977).
[41] Y. Q. Li, P. Davidovits, Q. Shi, J. T. Jayne, C. E. Kolb, and D. R. Worsnop, J. Phys. Chem. A **105**, 10627 (2001).
[42] I. M. Lifshitz and V. V. Slyozov, J. Phys. Chem. Solids **19**, 35 (1961).
[43] P. J. Robinson and K. A. Holbrook, *Unimolecular Reactions* (Wiley, New York, 1972).
[44] J. A. Miller and S. J. Klippenstein, J. Phys. Chem. A **108**, 8296 (2004).
[45] L. A. Curtiss, D. J. Frurip, and M. Blander, J. Chem. Phys. **71**, 2703 (1979).
[46] S. M. Kathmann, G. K. Schenter, and B. C. Garrett, J. Chem. Phys. **111**, 4688 (1999).